TEM studies of microstructural evolution in creep exposed E911

G. Qin[1], S.V. Hainsworth[1], A. Strang[1], P.F. Morris[2] P.D. Clarke[2] and A.P. Backhouse[3]

[1] Department of Engineering, University of Leicester, University Road, Leicester, LE1 7RH, UK

[2] Corus Research, Development and Technology, Swinden Technology Centre, Moorgate, Rotherham, S60 3AR, UK

[3] Corus Engineering Steels, Aldwarke Lane, Rotherham, South Yorkshire, S60 1DW, UK

Abstract

Transmission electron microscopy has been used to investigate precipitate evolution in E911 steel samples creep tested to a range of temperatures (600-650˚C) for durations of up to 75,000 hours. E911 is a 9%Cr 1% MoNbVNW creep resistant ferritic/martensitic steel that is used for boiler applications in power generation plant.
The initial microstructure consists of tempered martensite containing $M_{23}C_6$ precipitates at the prior austenite and martensite grain boundaries together with fine M_2X and MX precipitates in the matrix. A small amount of primary MX is also observed within the matrix. After prolonged exposure at high temperature and stresses, coarsening of the original M_2X and $M_{23}C_6$ was found to occur together with the precipitation of Laves phase and Z-phase. The paper discusses the evolution of the microstructure and relates this to the hardness and strength changes observed owing to creep testing of the alloy.

Keywords: TEM, E911, Laves phase, M_2X phase, Z phase, $M_{23}C_6$

1.Introduction

E911 is a 9%Cr1%MoNbVNW ferritic/martensitic steel that was originally developed in the European COST programme [1, 2] for power generation plant boiler, pipe and tube applications in steam driven power generation plant [3].

In the normalised 1100˚C and tempered 760˚C condition of E911, the microstructure consists of tempered martensite. The general microstructure consists of prior austenite (γ) grains containing martensite packets, blocks and laths as shown schematically in figure 1 and annotated on the microstructure shown in figure 2.

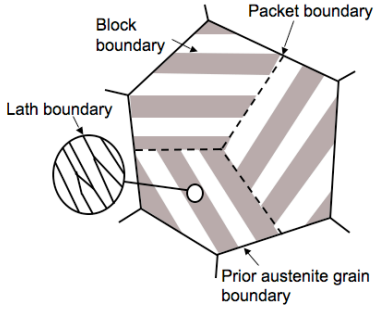

Figure 1: Schematic diagram of the martensite microstructure

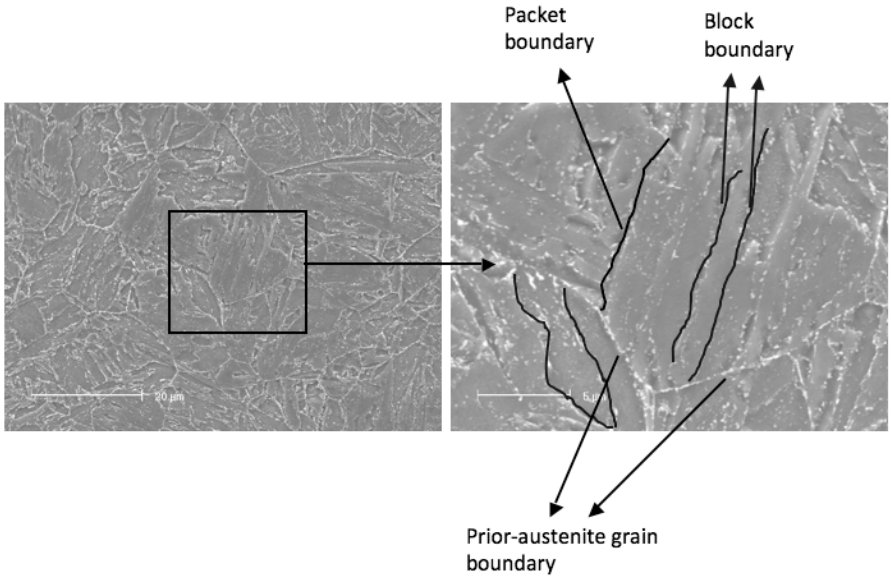

Figure 2: Scanning electron micrographs of the martensite microstructure showing the prior-austenite grain boundaries, packet boundaries and block boundaries.

E911 steel is strengthened by both solid solution and precipitation strengthening mechanisms with Cr, Mo and W primarily contributing to solid solution strengthening and other elements Nb, V and N contributing to the formation of precipitates which act to improve strength and limit grain size. In the normalised and tempered condition, $M_{23}C_6$ precipitates occur on the prior austenite and martensite lath boundaries together with finer V and Nb rich carbonitrides precipitated within the grains (M_2X and MX type precipitates). At the lath boundaries, the $M_{23}C_6$ particles are typically 0.10-0.17μm in size and the precipitates pin the grain boundaries and help to maintain a high dislocation density and stabilise the microstructure. At high temperatures, the $M_{23}C_6$ precipitates coarsen due to Oswald ripening thus reducing grain boundary pinning which leads to recovery and grain growth with corresponding reductions in dislocation densities. The other main precipitates, which have the greatest effect on precipitation strengthening, are typically fine (<0.1μm) VN and NbC (MX) type particles. The strength is maximised by ensuring that V and N are stoichiometrically balanced, this balancing is influenced by the presence of secondary chromium, iron and niobium in the precipitates. The VN precipitates have been found to be stable in size over long periods at 600˚C and 650˚C although over time Laves phase forms between 600 and 700˚C which removes W and Mo from the solid solution. When Laves phase grows in service, it evolves to large particles (0.5-1μm) and gives no additional strength and can decrease ductility [4, 5].

The presence of Z phase precipitates in a number of different 9% Cr steels at 600°C has been investigated by Sawada [6]. Danielsen and Hald [7] showed that Cr has a strong influence on the precipitation of Z phase with higher Cr contents allowing Z phase to be formed more rapidly while the work by Vodarek and Strang [5] has shown that Ni contents have a role in the precipitation of Z-phase. Vodarek and Strang [5] also showed that Z-phase was precipitated on primary NbC precipitates suggesting that niobium is important for Z-phase nucleation. This has been further confirmed more recently by Golpayegani *et al* [8]. Z phase is a large particle which does not contribute to precipitation strengthening. The formation of Z phase in E911 is low. In E911 steel, when the Laves phase is precipitated at shorter creep durations, the initial effect is to provide higher creep resistance since the total volume fraction of the secondary phase rises and this can contribute to precipitation strengthening. At longer creep durations, the beneficial effect of Laves phase is reduced by particle coarsening.

The role of M_2X phase evolution was investigated by Chilukuru *et al* [9] who found that M_2X phase coarsens much faster than VX, forming large M_2X precipitates at subgrain boundaries at the expense of the M_2X precipitates in the subgrain interior. This reduces the effect of precipitation hardening of the subgrain interior.

Although there have been a number of reports on the precipitation behaviour of 9-12% Cr steel, there has not been a systematic study of precipitate evolution in E911 at 600, 625 and 650˚C which are the temperatures particularly relevant to power plant operation. In this paper, we report on the distribution, chemical composition and size evolution of Laves phase, $M_{23}C_6$ phase, M_2X phase and Z phase in E911 creep samples at 600°C, 625°C, 650°C.

2. Materials and Experimental Procedures

2.1 Materials

The material studied in this investigation was E911 supplied by Corus which had the composition outlined in table 1. Tubes of the material were solution heat treated for 1 hour at 1100˚C air cooled and then tempered at 760˚C for 2 hours and air cooled.

Standard creep-rupture specimens were machined from tube in the longitudinal direction. Creep rupture testing was conducted under varying stress levels at 600, 625 and 650˚C, the results of which are shown in Table 2.

Table 1: Chemical composition of E911 (wt%)

C	Si	Mn	P	S	Cr	Mo	Ni	V	Al	Nb	W	N	Cu	Ti
0.115	0.19	0.35	0.007	0.003	9.10	1.00	0.22	0.23	0.006	0.069	0.98	0.069	0.08	0.002

Table 2: Stress, temperature and duration for the 12 creep samples in this study

600ºC		625ºC		650ºC	
Duration (hrs)	Stress (MPa)	Duration (hrs)	Stress (MPa)	Duration (hrs)	Stress (MPa)
1614hrs	200	1131hrs	154	849hrs	124
9800hrs	154	5487hrs	124	2232hrs	108
13336hrs	139	13224hrs	108	4530hrs	93
75647hrs	108	31198hrs	93	14319hrs	77

The long-term creep data obtained for E911 inevitably shows a general reduction in creep resistance with increasing test temperature and exposure duration, at 600°C, the longest creep rupture life was 75647 hours at a stress of 108 MPa; however, at 625°C, the longest rupture life dropped down to 31198 hours at a stress of 93 MPa, at 650°C, even down to 14319 hours at a stress of 77 MPa.

2.2 Sample preparation

Carbon replicas for examination in the transmission electron microscope were obtained from the middle of the head and the middle of gauge length of the creep exposed samples.

The procedure for preparing carbon replicas was to initially grind the samples flat using 240, 400, 600, 800 and 1000 grit papers (1 minute per step) and then polish with 6µm, 3µm, and 1µm diamond suspensions for 10 minutes each. After polishing the samples were initially etched with Vilellas etchant (1% picric acid and 5% hydrochloric acid in ethanol) until the surface was matt, and no reflections could be seen. A carbon film ~20 nm thick was then deposited by carbon evaporation at about 1700 ms with a pressure of $\sim 1 \times 10^{-3}$ Pa. The coating surface was then lightly scored into squares of 3 mm side length. Thereafter, the bulk material was immersed in Vilella's reagent again until the replicas lifted by metal dissolution, this procedure lasted 1-2 hours for long creep exposure samples and about 30 minutes for short creep duration samples. Finally, the replicas were repeatedly cleaned in 10% methanol in deionised water and collected on nylon grids.
TEM analysis was conducted in a JEOL 2100 LaB_6 filament transmission electron microscope (TEM). Images were acquired on a Gatan 2k x 2k digital camera and a PGT Avalon EDX system was used for X-ray analysis.

3. Results and Discussion

3.1 As-received microstructure

The as-received sample showed a characteristic tempered martensitic microstructure with a dispersion of $M_{23}C_6$ precipitates at prior austenite and martensite lath boundaries. Fine M_2X and MX carbonitride precipitates (e.g. NbC and VN type) were also observed within the laths by FEGSEM. The hardness of the as- received sample was measured to be 269 Hv ± 2.4 Hv. The average size of the prior-austenite grains was found to be 20.2 µm. Figure 3a shows the typical precipitate distribution for the as-received sample and Figure 3b shows a corresponding selected area diffraction pattern for one of the $M_{23}C_6$ particles.

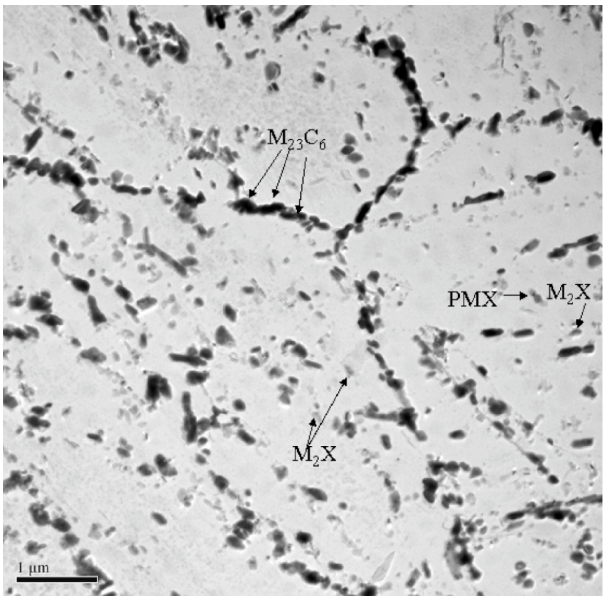

Figure 3a: TEM micrograph of the precipitate distribution in the 'as-received' solution treated and tempered E911.

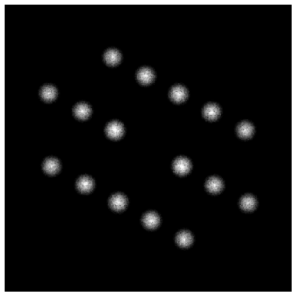

Figure 3b: Selected area diffraction pattern of an $M_{23}C_6$ particle (inverted image). Zone axis [-12-2]

For the 'as-received' sample, the majority of the precipitates observed are $M_{23}C_6$, MX and M_2X phase. Occasionally, primary MX phase particles were identified. No Laves phase was present. The mean size of M_2X particles is 166±10 nm in length, 60±6 nm in width. The MX particles are < 100 nm in size.

3.2 Effect of creep exposure on mechanical properties

Vickers hardness testing was performed on the head and gauge length of the creep exposed samples. Figure 4 shows the hardness data obtained for the samples investigated.

After creep exposure, the hardness decreases in both the head and the gauge length compared to the 'as-received' solution treated and tempered sample. The decrease in hardness is more significant in the gauge length owing to the accumulation of creep strain in this region whereas it can be assumed that the head is essentially strain free. The data points show the average hardness measured in the head and the gauge length of the fractured samples plotted against the Larson-Miller Parameter (LMP) with a constant (C) of 20 (where T is the temperature in degrees centigrade and t is the time to creep-rupture in hours). The Larson-Miller Parameter was calculated taking into account the initial tempering heat treatment of 2 hours at 760˚C in combination with the creep exposure time and temperature.

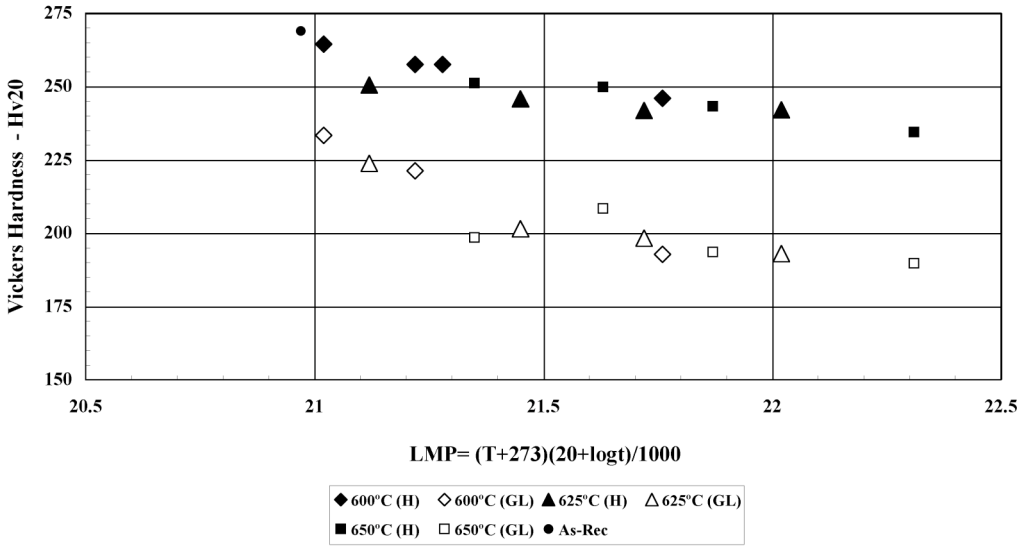

Figure 4: Vickers hardness against Larson-Miller parameter for the creep-exposed samples. H and GL denote head and gauge length respectively.

3.3 Creep exposed microstructures

The size, chemistry and morphology of the precipitates forming in the creep exposed samples have been investigated using transmission electron microscopy of carbon extraction replicas.

Figure 5 shows bright field TEM carbon extraction replicas from the head parts of the specimens that were creep exposed to differing durations at 600, 625 and 650˚C. Figure 5a shows Laves phase particles distributed along prior austenite grain boundaries and packet boundaries. M_2X and $M_{23}C_6$ particles were distributed along the lath boundaries, packet boundaries and prior austenite grain boundaries. This specimen was exposed to the lowest temperature for a short duration and Laves phase has appeared even after this short time. Figure 5b shows a replica from a specimen exposed at 600˚C for 75647 hours. The Laves phase particles have coarsened from the particles seen in figure 5a. Figures 5c and 5d show specimens exposed at 625˚C. Again Laves phase is present in both the short duration and longer duration samples. Figures 5e and 5f show TEM micrographs of the specimens exposed at 650˚C. It is noticeable that the density of small particles in the replicas is much reduced as compared to figures 5a-d and this accounts for the reduction in hardness that was seen in figure 4 as the precipitates no longer pin dislocations in the structure.

The Laves phase particles nucleated on the site of $M_{23}C_6$ as can be seen in figure 6a. Figure 6b shows the corresponding EDX analysis for this particle confirming the chemistry is consistent with Laves phase. Considerable particle coarsening was observed for the Laves phase particles over the samples

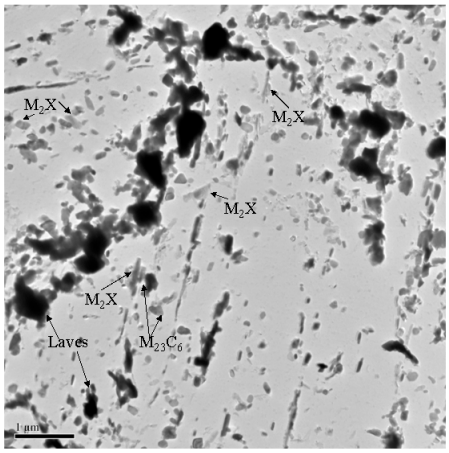

Figure 5a: 600°C 9800 hours head

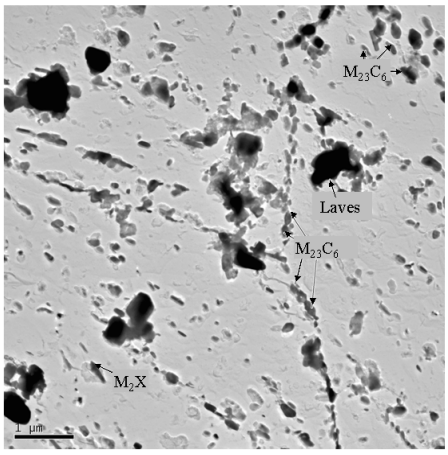

Figure 5b: 600°C 75647 hours head

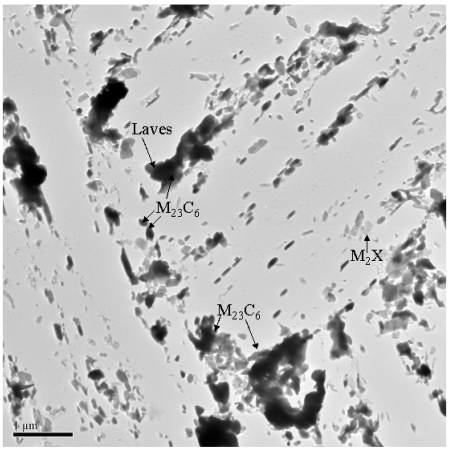

Figure 5c: 625˚C 1132 hours head

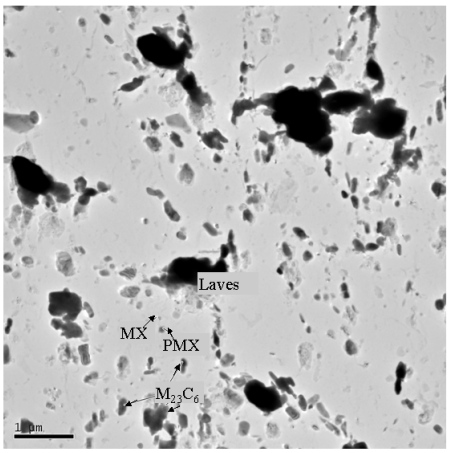

Figure 5d: 625˚C 31198 hours head

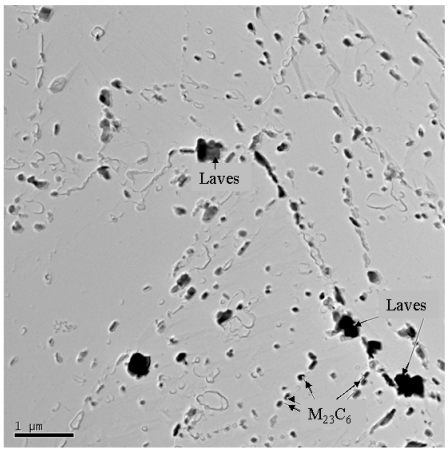

Figure 5e: 650˚C 849 hours head

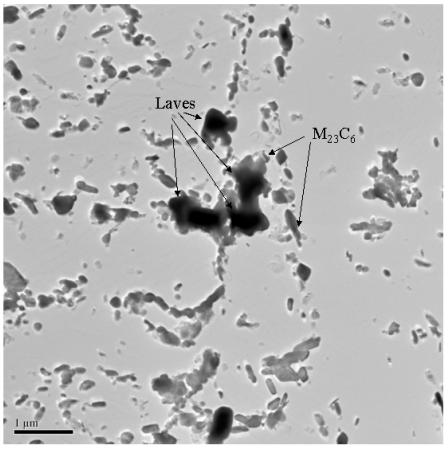

Figure 5f: 650˚C 14319 hours head

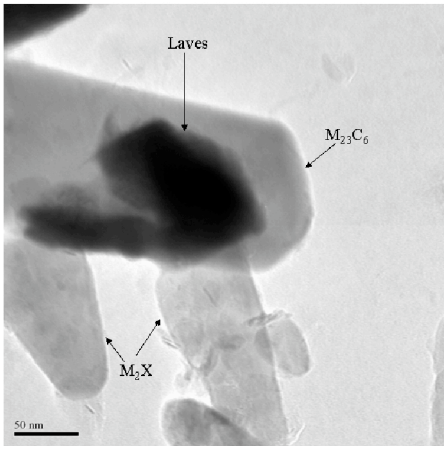

Figure 6a: Laves phase nucleation in the head of the sample exposed at 600°C for 1614 hours.

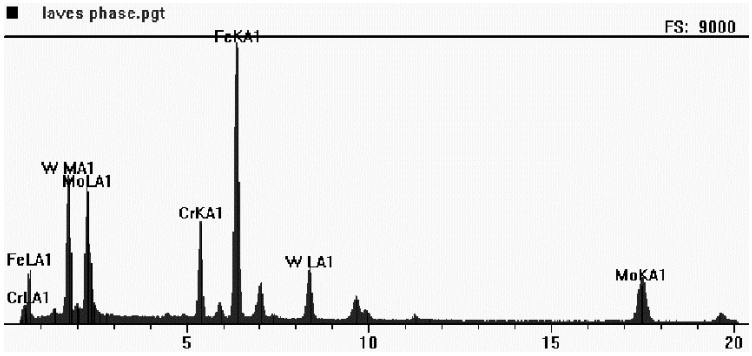

Figure 6b: EDX analysis of Laves phase particle in figure 5a.

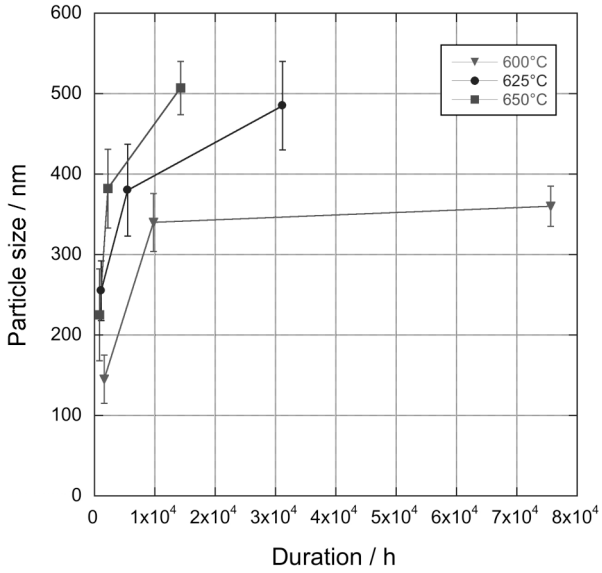

Figure 7a: Average Laves particle sizes as a function of exposure in the heads of the specimens

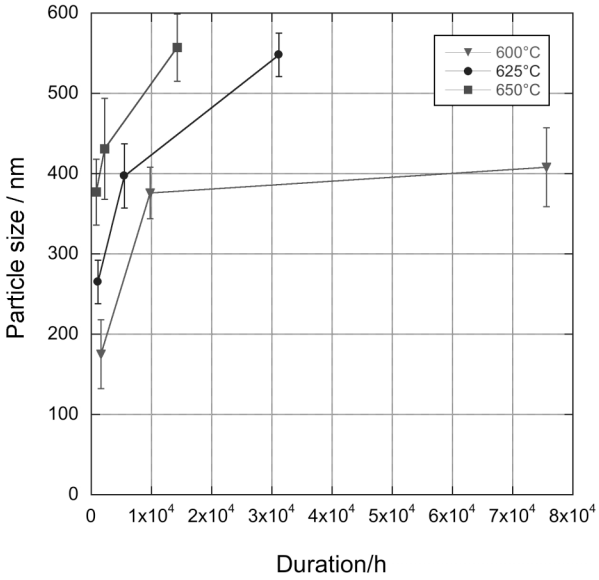

Figure 7b: Average Laves particle sizes as a function of exposure in the gauges of the specimens

studied. Figures 7a and 7b show the typical particle sizes as a function of creep duration at the differing temperatures studied for the head and gauge respectively.

TEM micrographs of the typical precipitate evolution in the gauge are shown in figure 8 a-f. Similar particle distributions were found in the gauges to the head but particle sizes were larger and coarsened to a greater extent as can be seen by comparing the sizes of Laves phase particles in the head and gauge shown in figure 7.

M_2X phase was found for all samples including the 'as-received' sample. M_2X has a hexagonal close packed crystal structure [9]. After exposure to stress and temperature the morphology of the particles changed quite considerably. Figure 9 shows the way in which the M_2X particles evolved with stress and temperature. In service, the shape of the M_2X samples gradually changed from needle-like (coherent) precipitates to more equiaxed morphologies (incoherent). The changes in coherency increases the interfacial energy and therefore increases the coarsening rate [9]. The behaviour of M_2X

in E911 is dissimilar to that observed in 12CrMoVNb steels by Vodarek and Strang [5] where the fine M_2X particles gradually dissolved, initially owing to the precipitation of (V,Nb)X phase which was a transient phase that itself dissolved to form Z phase.

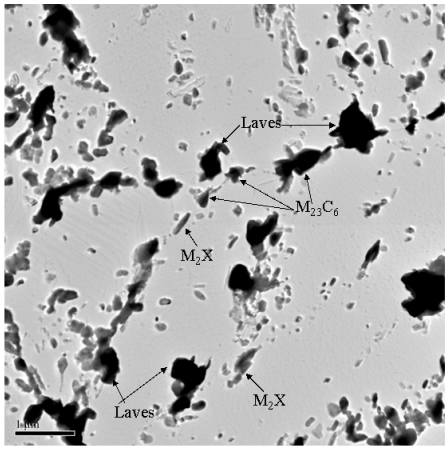

Figure 8a: 600˚C 9800 hours gauge

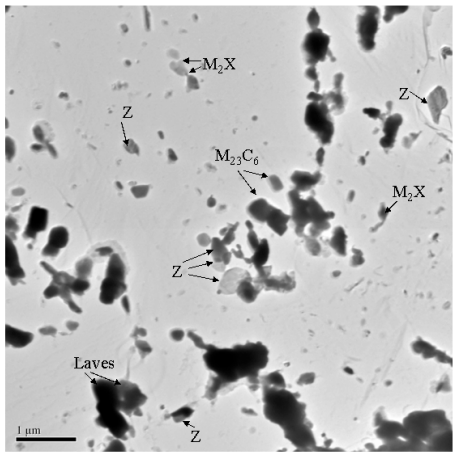

Figure 8b: 600˚C 75647 hours gauge

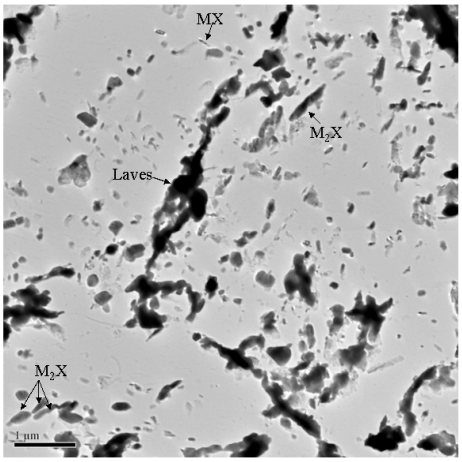

Figure 8c: 625˚C 1132 hours gauge

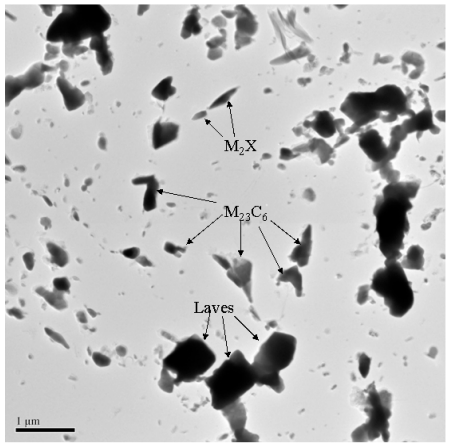

Figure 8d: 625˚C 31198 hours gauge

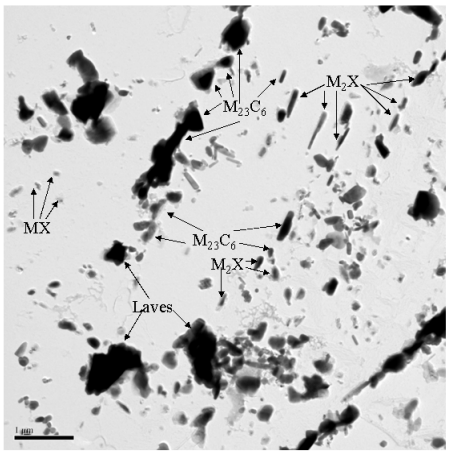

Figure 8e: 650˚C 849 hours gauge

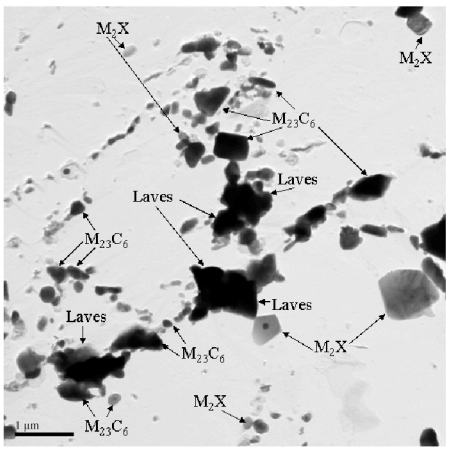

Figure 8f: 650˚C 14319 hours gauge

For MX particles, no coarsening was observed in any of the creep exposed samples. The MX phase was extremely stable over the range of samples investigated here. However, particle coarsening was observed for Laves phase, M_2X and $M_{23}C_6$ particles.

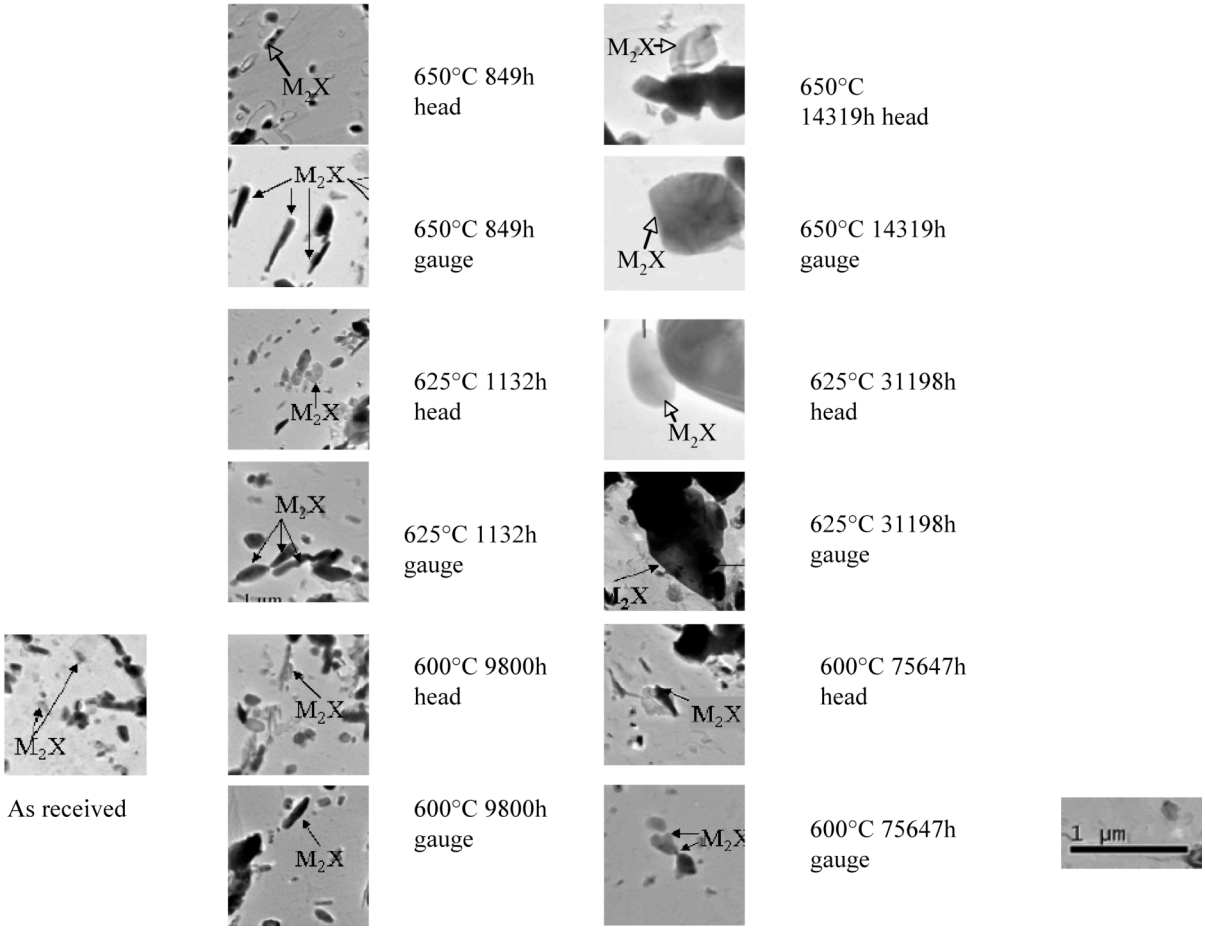

Figure 9: The effect of temperature and creep duration on the morphology and size of M_2X particles. After exposure to temperature and stress the particles evolve from an initally needle-like coherent morphology to a more equiaxed incoherent morphologies.

Z phase particles were found in the gauge of the sample exposed to the longest creep duration of 75647 hours. The Z phase particles were small, typically 280-320nm although some particles of around 450nm diameter were found.

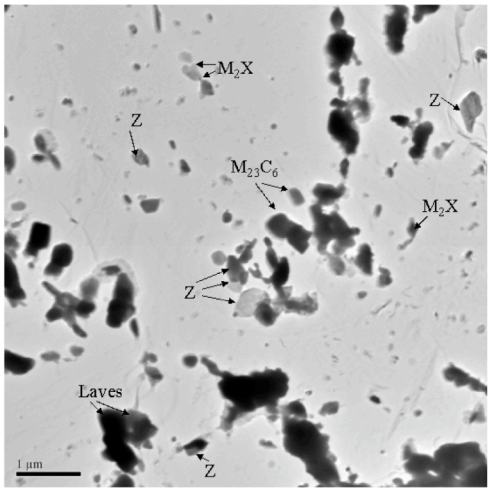

Figure 10a: TEM micrograph of Z-phase particles found in the gauge of the specimen exposed at 600˚C for 75647 hours

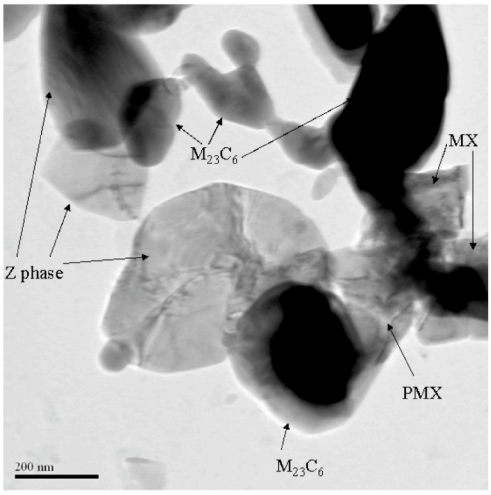

Figure 10b: Higher magnification TEM micrograph of the Z-phase particles

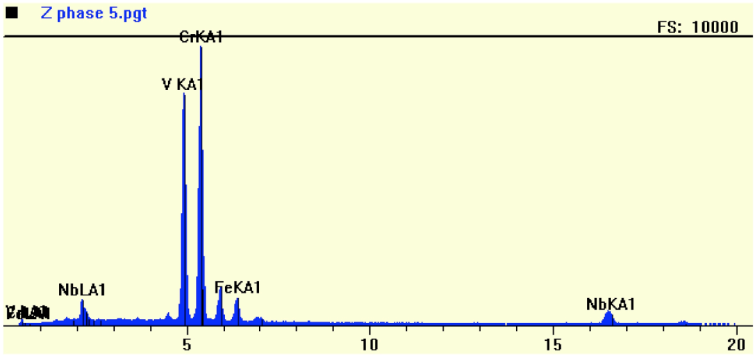

Figure 10c: EDX spectra showing the composition of the particles in figure 10b is consistent with Z phase.

Z phase is known to be deleterious to mechanical strength [5] and further work is on-going to investigate samples exposed to longer creep durations.

The observations of the changes in precipitate size and distribution here correlate with our previous studies of the change in the structure of E911 by EBSD. Our previous studies showed that changes in the low angle to high angle misorientation ratio occurred as the samples were exposed to stress and temperature [10]. At lower temperatures (600˚C), the low angle/high angle ratio was found to increase as a function of creep exposure whereas at higher temperatures (650˚C) the low angle/high angle ratio initially increased and then dropped as subgrain growth occurred. These changes in low angle/high angle ratio are consistent with the decrease in the effectiveness of precipitates in pinning the different grain boundaries in the martensite structure owing to the effects of both coarsening and dissolution and precipitation of larger particles in the matrix.

Conclusions

The hardness and creep strength of E911 steels decrease after long term creep exposure owing to changes in the microstructure. Detailed TEM investigations of creep-exposed E911 show that:

i. After even short term creep exposure, Laves phase was found to precipitate at packet and prior austenite grain boundaries

ii. $M_{23}C_6$ was distributed at lath boundaries, packet boundaries and prior austenite grain boundaries

iii. Z phase was found after long creep durations at 600˚C.

iv. No coarsening was found for MX particles but M_2X, $M_{23}C_6$ and Laves phase particles were found to coarsen as the temperature and time of exposure increased.

Acknowledgements

G. Qin thanks Corus and the EPSRC for support through the CASE studentship scheme. G. Clarke is thanked for his assistance with the microscopy.

References

[1] C. Berger, R.B. Scarlin, K.H. Mayer, D.V. Thornton, *et al*. "Steam turbine materials: high temperature forgings" in Materials for Advanced Power Engineering. 1994. Liege: Kluwer Academic Publishers. 47-72

[2] J. Orr and D. Burton. "Improving the elevated temperature strength of steel 91 (9%CrMoNbVN)" in Materials for Advanced Power Engineering. 1994. Liege: Kluwer Academic Publishers. 263-280

[3] P.J. Ennis. "The long-term creep rupture properties of 9-12%Cr steels" in Advances in Turbine Materials, Design and Manufacturing. 1997. Newcastle upon Tyne: The Institute of Materials. 296-308

[4] J. Hald, International Journal of Pressure Vessels and Piping 2008, **85,** 30-37

[5] V. Vodarek, A, Strang, Materials Science and Technology 2000, **16**, 1207-1213

[6] K. Sawada, H. Kushima, K. Kimura, ISIJ International, 2006, **46** , 769-775.

[7] H. Danielsen, J. Hald, Energy Materials, 2006, **1**, 49-57.

[8] A. Golpayegani, H.O. Andren, H. Danielsen, J. Hald, Materials Science and Engineering A 2008, **489**, 310-318

[9] H. Chilukuru, K. Durst, M. Goken, W. Blum, "On the roles of M_2X and Z-phase in tempered martensitic 9-12% Cr steels" in Materials for Advanced Power Engineering. 2006. Liege: Forschungszentrum Jülich GmbH Vol. **III** 1241-1250

[10] G. Qin, S.V. Hainsworth, P.F. Morris, P.D. Clarke, A.P. Backhouse & A. Strang "Effect of high temperature creep deformation on microstructural development of E911" Proceedings of the 7th International Charles Parsons Turbine Conference, Parsons 2007, Power Generation in an Era of Climate Change (Eds. A Strang, W.M. Banks, G.M. McColvin, J.E. Oakey, R.W. Vanstone) 2007 IOM Communications Ltd., London 441-452